Computational Fluid Dynamics (CFD) Analysis for the Reduction of Impeller Discharge Flow Distortion

R. Garcia and P. K. McConnaughey
Marshall Space Flight Center

A. Eastland
Rocketdyne Division, Rockwell International

Introduction

The use of CFD in the design and analysis of high performance rocket engine pumps has increased in recent years. This increase has been aided by the activities of the Marshall Space Flight Center (MSFC) Pump Stage Technology Team (PSTT) (table 1). The team's goals include assessing the accuracy and efficiency of several methodologies and then applying the appropriate methodology(s) to understand and improve the flow inside a pump. The PSTT's objectives, team membership, and past activities are discussed in Garcia[1] and Garcia[2]. The PSTT is one of three teams that form the NASA/MSFC CFD Consortium for Applications in Propulsion Technology (McConnaughey[3]). The PSTT first applied CFD in the design of the baseline consortium impeller. This impeller was designed for the Space Transportation Main Engine's (STME) fuel turbopump. The STME fuel pump was designed with three impeller stages because a two-stage design was deemed to pose a high developmental risk. The PSTT used CFD to design an impeller whose performance allowed for a two-stage STME fuel pump design (table 2). The availability of this design would have lead to a reduction in parts, weight, and cost had the STME reached production. One sample of the baseline consortium impeller (figure 1) was manufactured and tested in a water rig. The test data showed that the impeller performance was as predicted and that a two-stage design for the STME fuel pump was possible with minimal risk. The test data also verified another CFD predicted characteristic of the design that was not desirable. The classical "jet-wake" pattern at the impeller discharge was strengthened by two aspects of the design: by the high head coefficient necessary for the required pressure rise and by the relatively few impeller exit blades, 12, necessary to reduce manufacturing cost (figure 2). This "jet-wake" pattern produces an unsteady loading on the diffuser vanes and has, in past rocket engine programs, lead to diffuser structural failure. In industrial applications, this problem is typically avoided by increasing the space between the impeller and the diffuser to allow the dissipation of this pattern and, hence, the reduction of diffuser vane unsteady loading. This approach leads to small performance losses and, more importantly in rocket engine applications, to significant increases in the pump's size and weight. This latter consideration typically makes this approach unacceptable in high performance rocket engines.

After all, one of the motivations for designing the baseline consortium impeller was to reduce pump weight. The "jet-wake" pattern predicted and measured for the baseline impeller, while not totally unacceptable, would have necessitated thick diffuser vanes if the typical impeller diffuser gap of 3-5 percent of the impeller radius were to be maintained. The thicker diffuser vanes would entail a performance loss, and because of the STME's gas-generator engine cycle, performance losses in the turbopumps leads directly to engine performance losses. This is especially true of the fuel pump which absorbs approximately three times the horsepower of the LOX pump. Therefore, the new challenge for the PSTT became to design a high head coefficient impeller with low blade count and a minimized blade to blade (b-t-b) velocity distortion.

To achieve this goal, it was decided that a parametric study should be conducted. This study consisted of evaluating the effect of six different geometric parameters on the impeller performance. The study included the participation of seven PSTT members using six different CFD codes. During the study the impeller designs analyzed had the same inlet and exit diameters and were designed to produce the same head as the baseline consortium impeller. This was done so that the effect of each parameter on the flow distortion could be adequately accessed. A listing of the cases analyzed appears on table 3. Each member performed an analysis of the baseline consortium impeller and the results of that analysis were used as the base of comparison for subsequent calculations. The grid sizes used were determined by each individual team member based on past experience with their code on impeller calculations. All the codes used have been previously benchmarked against two experimental Laser Velocimeter (L2F) datasets, most recently using data from the Space Shuttle Main Engine (SSME) High Pressure Fuel Turbopump (HPFTR) impeller tests (Brozowski[4]). These benchmark activities demonstrated that impeller performance and impeller exit flow distortion were predicted very well. Typical results are reported by Prueger[5] for the REACT3D code.

Figure 3 shows schematically the domain analyzed and the boundary conditions used in all but one case. In the actual hardware there is a rapid expansion in the flow area in the vaneless space between the impeller trailing edge and the diffuser vane leading edge. The affect of this vaneless space had been studied in the PSTT and it was found that ignoring it and instead modeling the passage as having a continuous width with "slip" boundaries was adequate for analyzing the impeller. However, to ensure that these earlier conclusions were applicable to the current design, one case was run of the baseline consortium impeller which included the actual vaneless space expansion downstream of the impeller. The inclusion of the vaneless space, while not changing the impeller flow significantly, did have a large effect on the velocity profiles at the radius corresponding to the diffuser vane leading edge. However, none of the calculations included the diffuser vanes or its potential effect on the impeller.

Results

The effect of a given parameter on the impeller performance was evaluated using both distributions of key performance variables and integrated "global" performance variables. Figure 4 shows the impact of the various parameter on the global head coefficient and efficiency. Figure 5 shows the effect on global distortion parameter. Ideally, the flow split should be equal on either side of the partial (or short) blades. Any mass flow imbalance across the partial blades will generate a dynamic load on the diffuser vanes. Not only should the flow be balanced on either side of the partial blade, but the velocity distribution in the b-t-b direction should be as uniform as possible. The b-t-b distortion parameter is a measure of the non-uniformity in the velocity in the b-t-b direction. Similarly, the hub-to-shroud (h-t-s) distortion parameter is a measure of the distortion of the flow vector in the h-t-s direction. Non uniformity in the h-t-s direction affects the design of the diffuser because it represents a spanwise flow angle variation to the diffuser vane. Small h-t-s distortions can be accounted for in the design but large distortions cannot. From figure 5 it can be seen that there is often an inverse relationship between b-t-b distortion and h-t-s distortion. Further, by comparing figures 4 and 5 it can be seen that distortion and efficiency are not necessarily proportional. One can have increased distortion and an accompanying increase in efficiency. Overall, most of the concepts studied did not significantly affect efficiency, which was very high on the baseline impeller, and only a few significantly changed the flow split, which was nearly ideal in the baseline impeller at 49 percent/51 percent. Therefore, the parameters studied changed the impeller exit distortion while preserving the desirable properties of the baseline consortium impeller. In the subsequent sections, each one of the six major geometric parameter variation grouping will be discussed.

Vaneless Space: Ames Research Center (ARC) was assigned the task of evaluating the effect of the actual vaneless space geometry immediately downstream of the impeller on the impeller performance. The geometry immediately downstream of the impeller was in all the other cases simplified by modeling it as a constant span area with slip boundary conditions. ARC was to perform an analysis to assess the validity of this simplification. ARC used the code INS3D-UP (Kiris[6]) to perform this task. Figure 6a shows that the h-t-s distribution is affected by the inclusion of the vaneless space but the form of the b-t-b distribution is not significantly affected (figure 6b). There is a slight increase in the work done by the impeller due to a delay in the blade trailing edge unloading that occurs when the vaneless space is included in the analysis.

Chordwise Blade Loading Distribution: Rocketdyne Division, Rockwell International (Rkdn) was assigned the task of evaluating the effect of changing the chordwise blade loading distribution on the impeller performance and distortion.

Rkdn used the CFD code REACT-3D (Chan[7]) to perform this task and the impeller axial length study to be discussed in the following section. The variations modeled where: (1) shifting the long blade's loading towards the leading edge, and (2) shifting the long blade's loading towards the trailing edge. Figure 8 shows that there was no clear change in the impeller's head coefficient and efficiency due to either one of these two changes. From figure 9 it is also evident that the b-t-b distortion was not significantly affected either. The low leading edge loading case does lead to a more favorable flow split (figure 5).

Impeller Axial Length: Rkdn also varied the impeller's axial length to determine its impact on performance and distortion. The baseline design has a low momentum region near the long blade leading edge along the shroud. It was proposed that an increase in the impeller's axial length would increase the radius of curvature and decrease or eliminate this low momentum region. For this portion of the study, the impeller's discharge axial width, B2, was decreased by 20 percent to reduce diffusion. Because of this latter change, the impeller blade exit angle was increaseed to 41.5 degrees from the baseline's 38 degrees to maintain a consistent head rise. Once again, the performance was not significantly affected by these changes (figure 8) but the b-t-b was decreased by the increased impeller axial length (figure 9). Note from figure 5, however, that the case with the lowest b-t-b distortion has the worst h-t-s distortion. Also, increasing the impeller axial length generally is a detriment to the rotordynamics of a pump. Therefore, if increasing the axial length of the impeller is used as a method for improving the baseline design, then considerations in addition to b-t-b distortion will weigh heavily on determining the definitive axial length.

Tandem Blading: SECA was assigned the task of evaluating the effect of cutting the long impeller blades near the leading edge and clocking one portion of the blade relative to the other. Earlier studies in the PSTT had indicated that tandem blades were to be successful, the cut of the long blade should be near the leading edge. SECA ran two cases where the tandem blades were rotated 7.5 degrees and 22.5 degrees, respectively, relative to the remainder of the long blade. This rotation was performed in the direction opposite to the impeller's rotation. The logic being to use high energy flow from the tandem blade's pressure side to energize the suction side of the long blade. SECA used the code FDNS3D (Chen[8]) to perform this task. The performance decreased significantly (figure 10) and the b-t-b distortion increased (figure 11). (Notice that because of the grid mapping, the angular reference is not the same for these three cases. This will be corrected for the final paper.) And these two changes suffered a double penalty in that the h-t-s distortion increased as well. The general conclusion is that small relative clockings may improve the flowfield, but large clockings do not. In retrospect, this concept may not be as effective as similar concepts are in other applications because the flow in a radial impeller is primarily dominated by rotational forces. The low momentum regions seen in the baseline design were caused by either the rapid bending of the streamline from the axial to

the radial direction or by the secondary flows set up by the pressure-to-suction pressure gradients.

Partial Blade Chord Length, Location: Location of the partial blade leading edge was also studied. Scientific Research Associates (SRA) studied two cases where the partial blade's chord length was increased. SRA used the code MINT (Briley[9]) to perform this task. Increasing the length of the partial increased the impeller exit b-t-b distortion (figure 12) as well as the h-t-s distortion (figure 5). Based on the trend in the flow split, a small increase in the partial blade length may provide the even mass split desired across the partial blade. The second portion of this part of the study involved maintained the partial blade's chord length constant, but varied the location of the partial's leading edge. In the baseline, the leading edge of the partial blade bisects the angle between adjacent long blade. For this task Lewis Research Center used the code HAH3d (Hah[10]). Initially, two variations about the baseline were run involving a 5 degree shift in the leading edge of the partial towards the suction side of the long blade, and a 5 degree shift towards the pressure side of the long blade. Based on these results, a third case involving a 2.5 degree shift towards the pressure side of the long blade was run. Figure 13 shows that the last two cases reduced the distortion in the b-t-b direction. The 2.5 degree shift has an ideal predicted flow split of 50/50. (The results of these calculations will be included in figures 4 and 5 of the final paper).

Blade Trailing Edge Lean: The trailing edge of the blades are nearly axial in the baseline design. Virginia Polytechnic Institute (VPI) studied the effect of varying the blade trailing edge circumferential location from h-t-s. Backward lean is defined as the shroud trailing edge leading the hub trailing edge as the impeller rotates. Forward lean is the reverse; the hub trailing edge leads the shroud trailing edge. The initial results indicated that backward lean did significantly reduce b-t-b distortion. However, the initial lean cases modeled also changed the blade trailing edge angle. Therefore, to understand whether it was the backward lean or the blade exit angle distribution that lead to the improvement, two additional cases were run which studied these two variations independently. Figure 14 shows that the backward blade lean is the dominant cause for the decrease of b-t-b distortion and from figure 5 it appears that a combination of blade lean and blade exit angle variations may be more effective than lean alone (VPI #2 vs. VPI #5). This concept looks promising but presents two potentially negative aspects: (1) the h-t-s distortion rises proportionally to the decrease in b-t-b distortion, and (2) the blade lean concepts may be more difficult to manufacture.

Conclusions

The PSTT has, with the use of CFD, improved the performance of rocket engine impellers. An example of the baseline consortium impeller has been tested and its

performance is very close to that predicted. Further studies have been conducted with the goal of arriving at design concepts which decrease the b-t-b flow distortion at the impeller exit without sacrificing performance. Results indicate that the simplifications made in the vaneless space downstream of the impeller do not compromise the results. Changing the work distribution along the blade chord did significantly affect the distortion. Small relative clockings in a tandem blade design may be beneficial as well as small increases in the chord length of the partial blade. Large clockings or large increases in the partial blade chord length tend to increase distortion. Changing the circumferential location of the partial blade leading edge, increasing the impeller axial length, and backward lean of the blade trailing edge are viable concepts for reducing the b-t-b distortion. These results will be studied in detail and a new impeller incorporating one or several of these concepts will be designed, manufactured, and tested. Based on the preliminary assessment of the results, the team has already decided that further increases in head coefficient are possible while still maintaining efficiency and acceptable levels of distortion.

References

1. Garcia, R., Jackson, E. D., and Schutzenhofer, L. A., "A Summary of the Activities of the NASA/MSFC Pump Stage Technology Team," Proceedings of the Fourth International Symposium on Transport Phenomena and Dynamics of Rotating Machinery, April 5-8, 1992, Honolulu, Hawaii.

2. Garcia, R., McConnaughey, P., and Eastland, A., "Activities of the Marshall Space Flight Center Pump Stage Technology," AIAA 92-3222, AIAA/SAE/ASME/ASEE 28th Joint Propulsion Conference, July 6-8, 1992, Nashville, TN.

3. McConnaughey, P. K. and Schutzenhofer, L. A., "Overview of the NASA/MSFC CFD Consortium for Applications in Propulsion Technology," AIAA 92-3219, AIAA/SAE/ASME/ASEE 28th Joint Propulsion Conference, July 6-8, 1992, Nashville, TN.

4. Brozowski, L. and Rojas, L., Paper discussing results of SSME HPFTP impeller testing, to be presented at the ASME 1993 Fluid Engineering Conference, June 21-24, 1992, Washington, DC (complete reference to be available for the final manuscript).

5. Prueger, G. and Eastland, A., Paper comparing CFD results to test data for the SSME HPFTP impeller, to be presented at the AIAA/SAE/ASME/ASEE 29th Joint Propulsion Conference, July 1993, Monterey, CA (complete reference to be available for the final manuscript).

6. Kiris, C., Rogers, S., Kwak, D., Chang, I., "Computational Approach for Probing the Flow Through Artificial Heart Devices," December 1991, Advances in Bioengineering, ASME Bioengineering Division, Winter Annual Meeting.

7. Chan, D. C. and Tran, K., "Turbulent Flow Analysis of a Double Circular Arc Compressor Cascade," AIAA 89-2569, AIAA 25th Joint Propulsion Conference.

8. Chen, Y. S., "Compressible and Incompressible Flow Computations with a Pressure Based Method," AIAA 899-0286, AIAA 27th Aerospace Sciences Meeting, January 9-12, 1989, Reno, Nevada.

9. Briley, W. R., et al, "Computational Flow Past a Turbine Blade with and without Tip Clearance," ASME Paper 91-GT-56, International Gas Turbine and Aeroengine Congress, Orlando, FL, June 1991.

10. Hah, C., Bryans, A. C., Moussa, Z., Tomsho, M. E., "Application of Viscous Flow Computations for Aerodynamic Performance of Backswept Impeller at Viscous Operating Conditions," Journal of Turbomachinery Trans. ASME, Vol. 110, pp. 303-311, July 1988.

Definition of Performance Parameters

$c_u = C_u / U_{tip}$ where C_u = absolute tangential velocity

$c_m = C_m / U_{tip}$ where C_m = meridional velocity

U_{tip} = wheel tip velocity

β = relative flow angle, in degrees, referenced from tangential dir.

α = absolute flow angle, in degrees, referenced from tangential dir.

η = efficiency - head rise/Euler head rise

Ψ = head coefficient - $\Delta H_t g / U_{tip}^2$

RSHL = rotor stagnation head loss coefficient

= (Euler head - head rise) g/U_{tip}^2

$$\text{Relative Radius} = (R_i - R_{hub}) / (R_{shroud} - R_{hub})$$

$$\text{Relative X} = (X_i - X_{shroud}) / (X_{hub} - X_{shroud})$$

$$\text{Relative Angle} = (\text{Angle}_i - \text{Angle}_{suction}) / (\text{Angle}_{pressure} - \text{Angle}_{suction})$$

Distortion Parameter Definitions

$$\text{hub-to-shroud} = [\max(\alpha_k) - \min(\alpha_k)]_{\text{hub-to-shroud}}$$

where α_k = mass averaged flow angle, averaged in the blade-to-blade direction

$$\text{blade-to-blade} = \bar{C}^2[\max(\alpha_j) - \min(\alpha_j)]_{\text{blade-to-blade}}$$

where $\bar{C}$ = average total discharge velocity

α_j = mass averaged flow angle, averaged in the hub-to-shroud direction

TABLE 1. PUMP TEAM MEMBERS

- NASA Marshall Space Flight Center (MSFC)
- NASA Ames Research Center (ARC)
- NASA Lewis Research Center (LeRC)
- David Taylor Research Center
- Rocketdyne (RDYN)
- Pratt & Whitney (P&W)
- Aerojet
- Ingersoll-Rand
- CFD Research Corporation
- SECA
- Scientific Research Associates (SRA)
- The University of Alabama in Huntsville (UAH)
- Pennsylvania State University (PSU)
- University of Cincinnati
- Virginia Polytechnic Institute
- California Institute of Technology

TABLE 2 - IMPELLER SPECIFICATION

RPM	30108
Impeller InletTip D	9.38
Impeller Inlet Hub D	6.097
Impeller Inlet ß	17.9
Impeller Outlet D	14.14
Impeller Outlet ß	38.0
Impeller B_2 Width	1.12
Impeller Tip Speed	1857
Impeller Specific Speed	1141
Impeller W_2/W_1	0.690
Impeller C_2/C_1	0.377
Impeller Cu_2/U_2	0.726
Impeller Blade Number	6+6

D: Diameter in Inch, ß: RMS Blade Angle from Tangential.

Table 3. List of Cases Analyzed

Cases Postprocessed

Organization	Size	Description
ARC #1	328K	Baseline
ARC #2	540K	Baseline with exit cavity at imp. exit
Rkdn #1	20K	Baseline
Rkdn #2	20K	Baseline envelope, heavy l.e. loading
Rkdn #3	20K	Baseline envelope, light l.e. loading
Rkdn #4	20K	Axial length +37%, B2 -20%, Beta2 = 41.5
Rkdn #5	20K	Axial length +20%, B2 -20%, Beta2 = 41.5
Rkdn #6	20K	Axial length +00%, B2 -20%, Beta2 = 41.5
SECA #1	71K	Baseline
SECA #2	75K	Tandem blade, 7.5 degrees clocking against rotation
SECA #3	75K	Tandem blade, 22.5 degrees clocking against rotation
SRA #1	160K	Baseline
SRA #2	160K	Increases partial blade length
SRA #3	160K	Longest partial blade length
VPI #1	33K	Baseline
VPI #2	20K	Backward blade lean, Moore distribution
VPI #3	20K	Forward blade lean, Moore distribution
VPI #4	33K	Base. envelope, no blade lean, Beta2 46-32 degrees
VPI #5	33K	Base. envelope, backward blade lean, Beta2 = 38 degrees

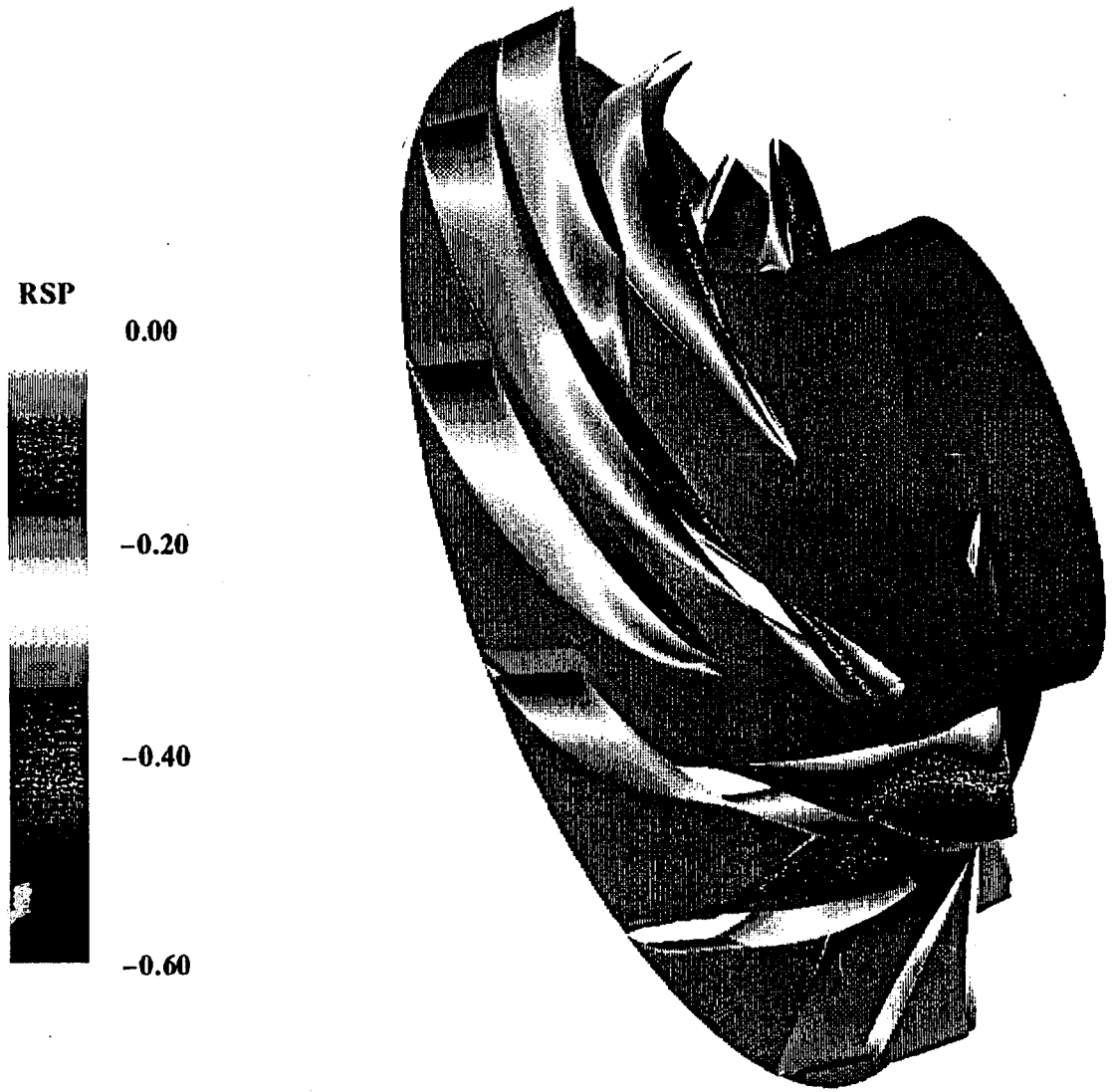

blade surfaces colored by Reduced Static Pressure (RSP)

Figure 1. Baseline Consortium Impeller

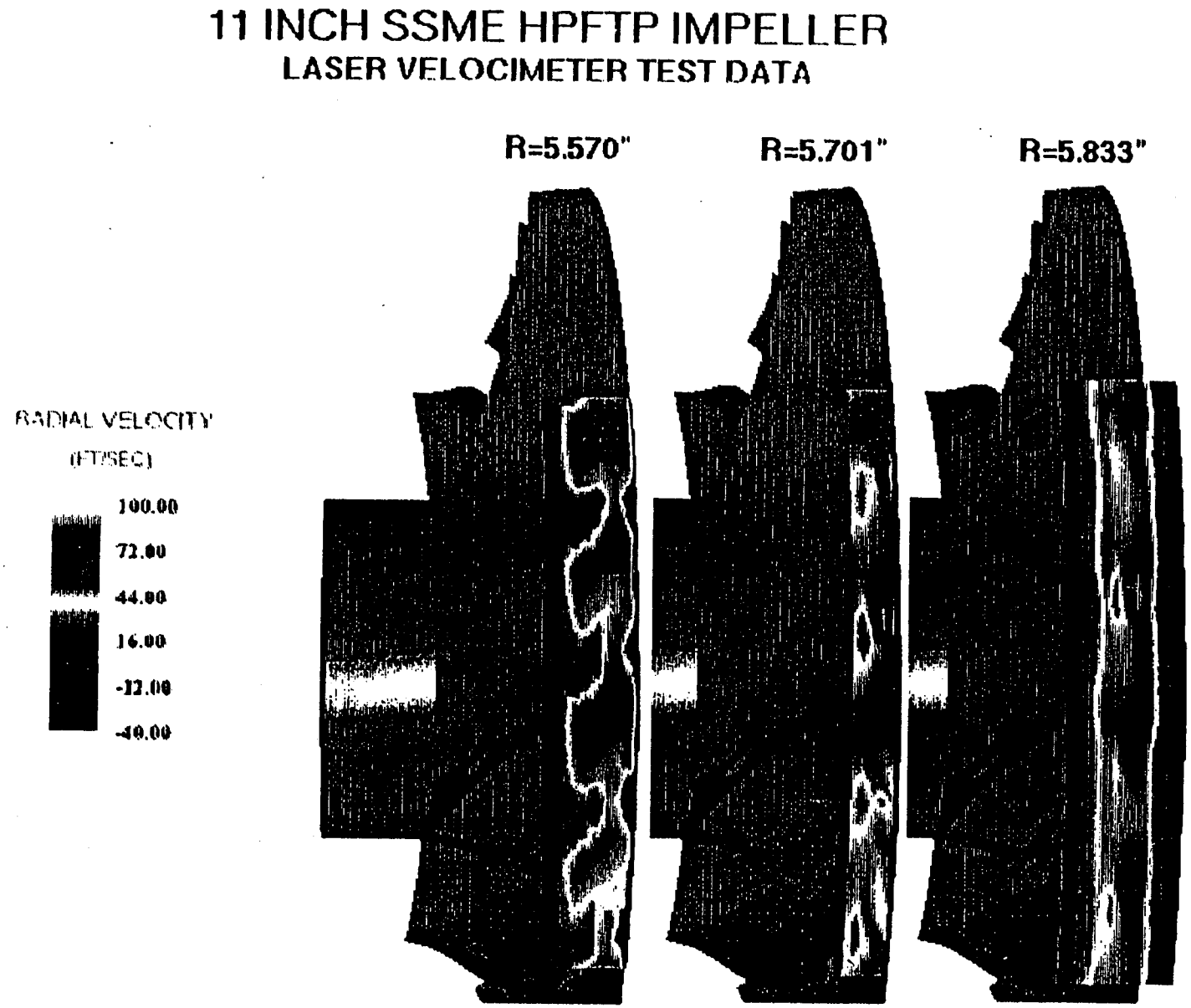

Figure 2. SSME HPFTP impeller exit radial velocity measurements

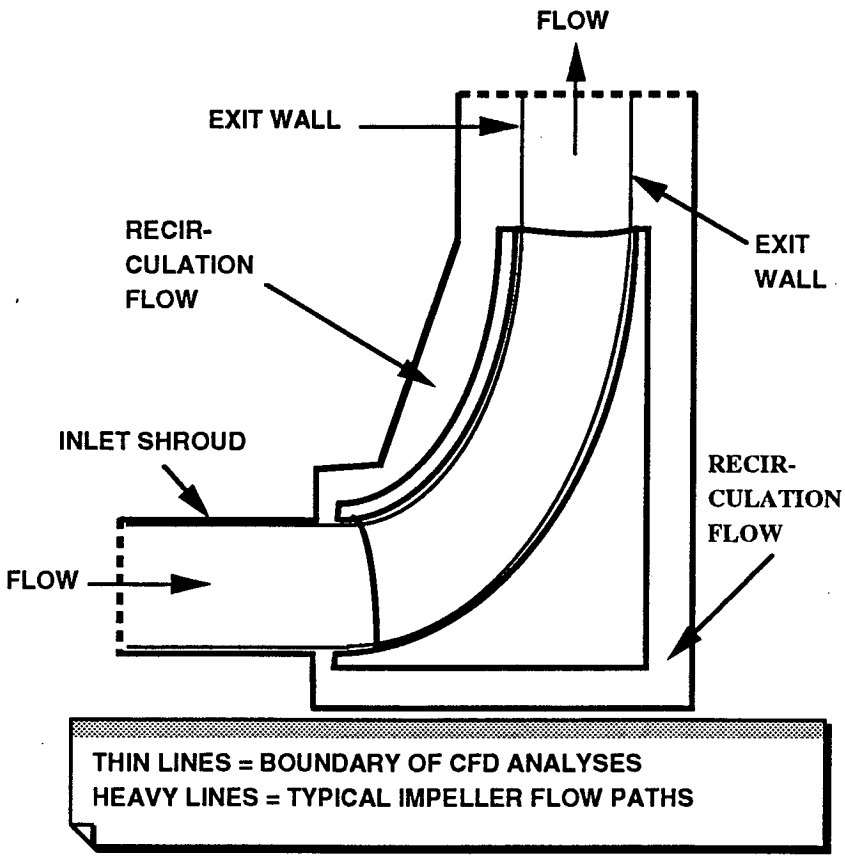

FIG. 3. SCHEMATIC OF IMPELLER GEOMETRY AND DOMAIN ANALYZED

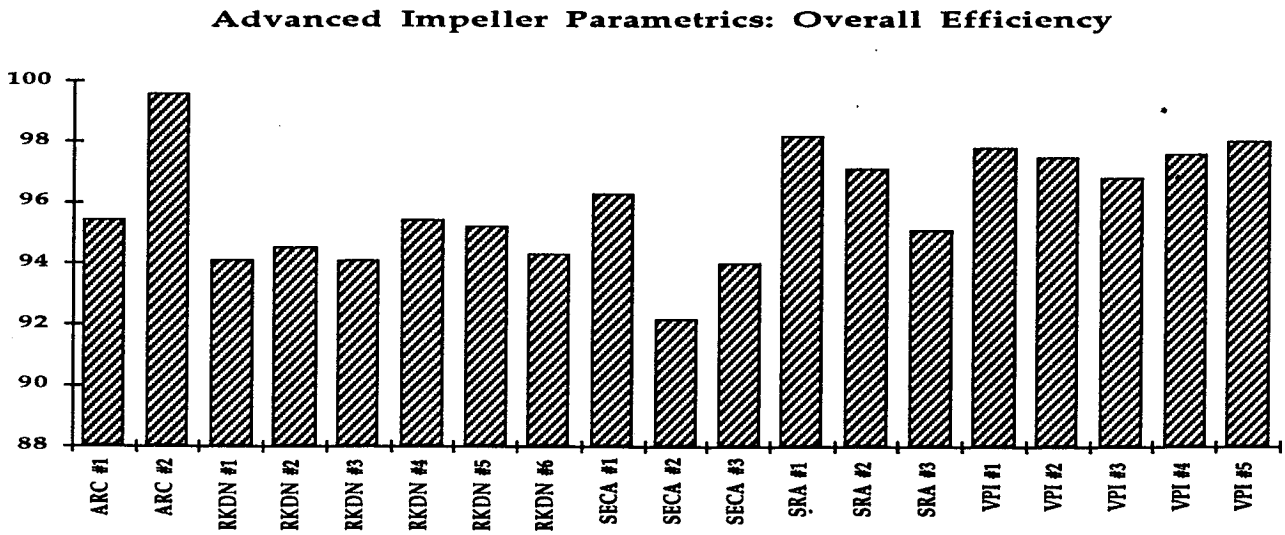

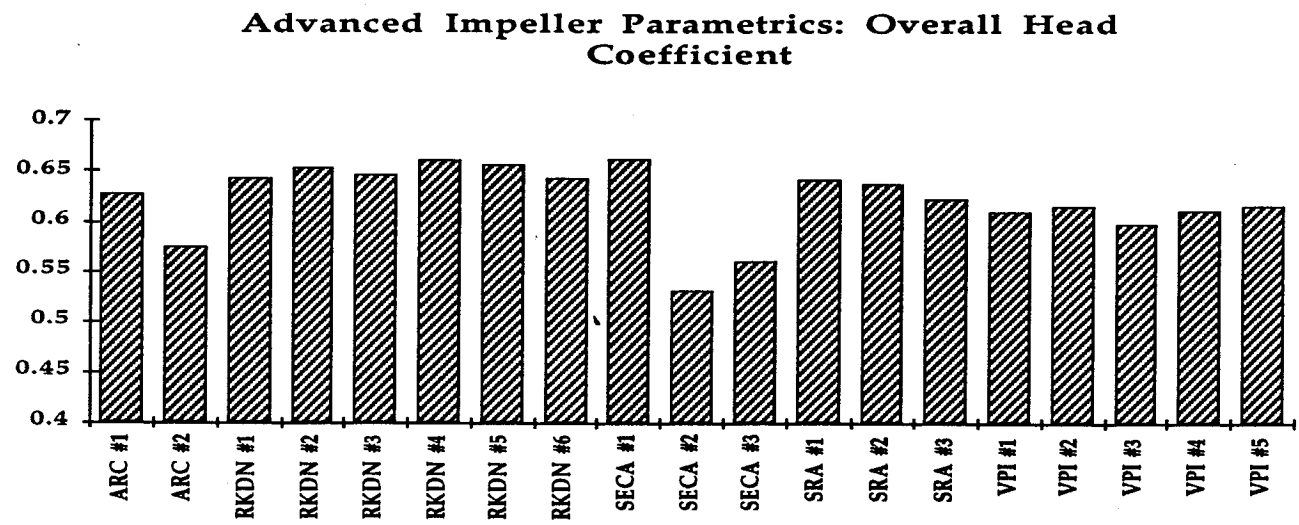

Figure 4. Integrated Impeller Performance Predictions

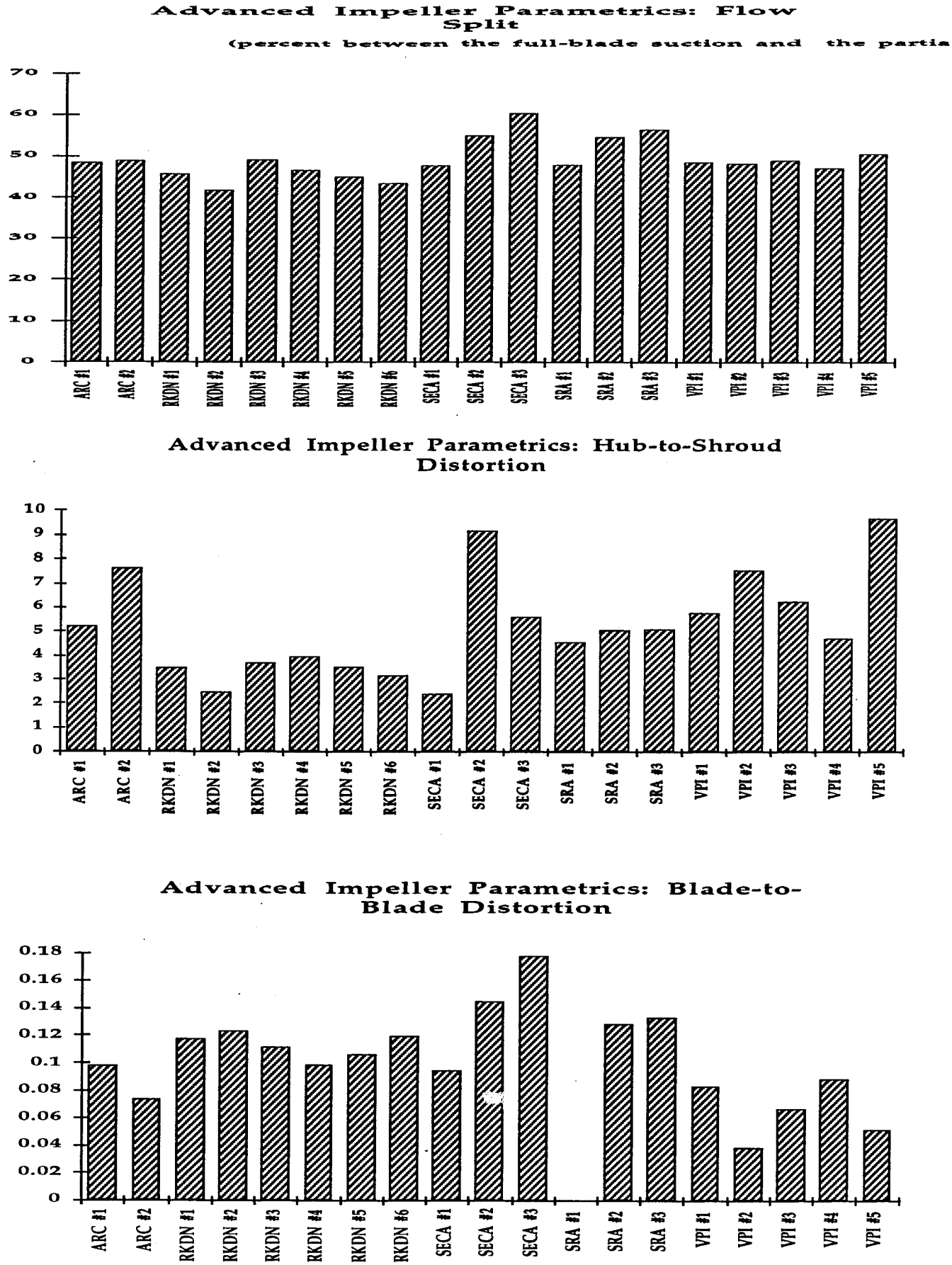

Figure 5. Integrated Impeller Exit Distortion Parameters

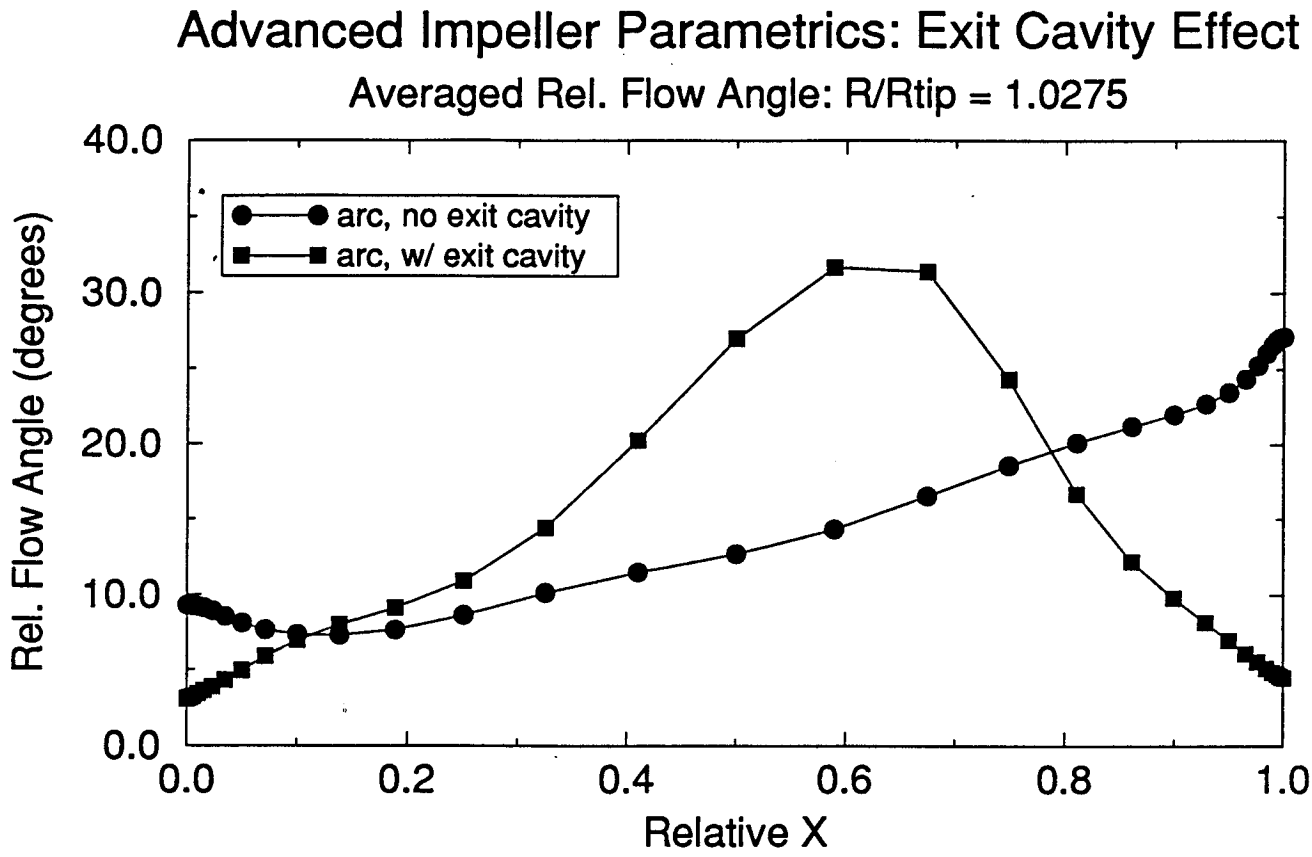

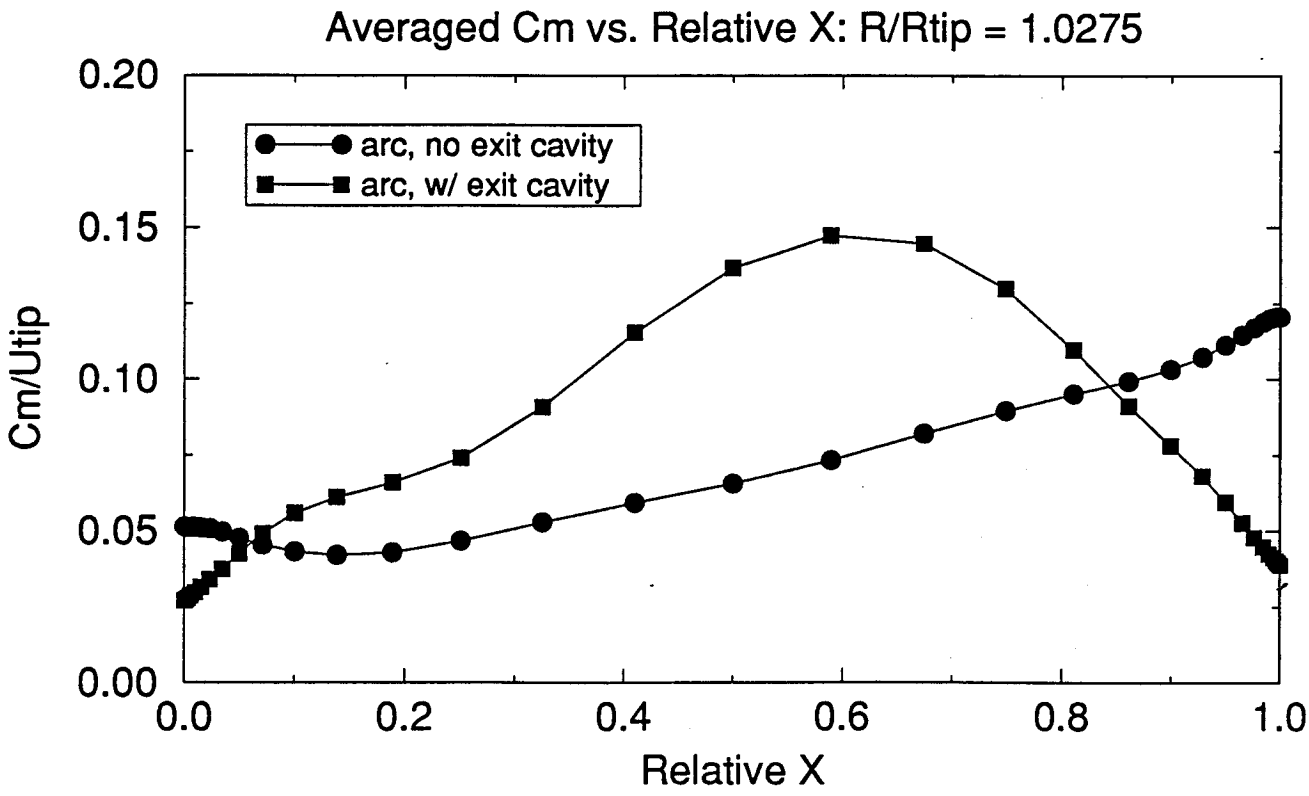

Figure 6a. Circumferentially averaged hub-to-shroud impeller exit radial velocity distribution

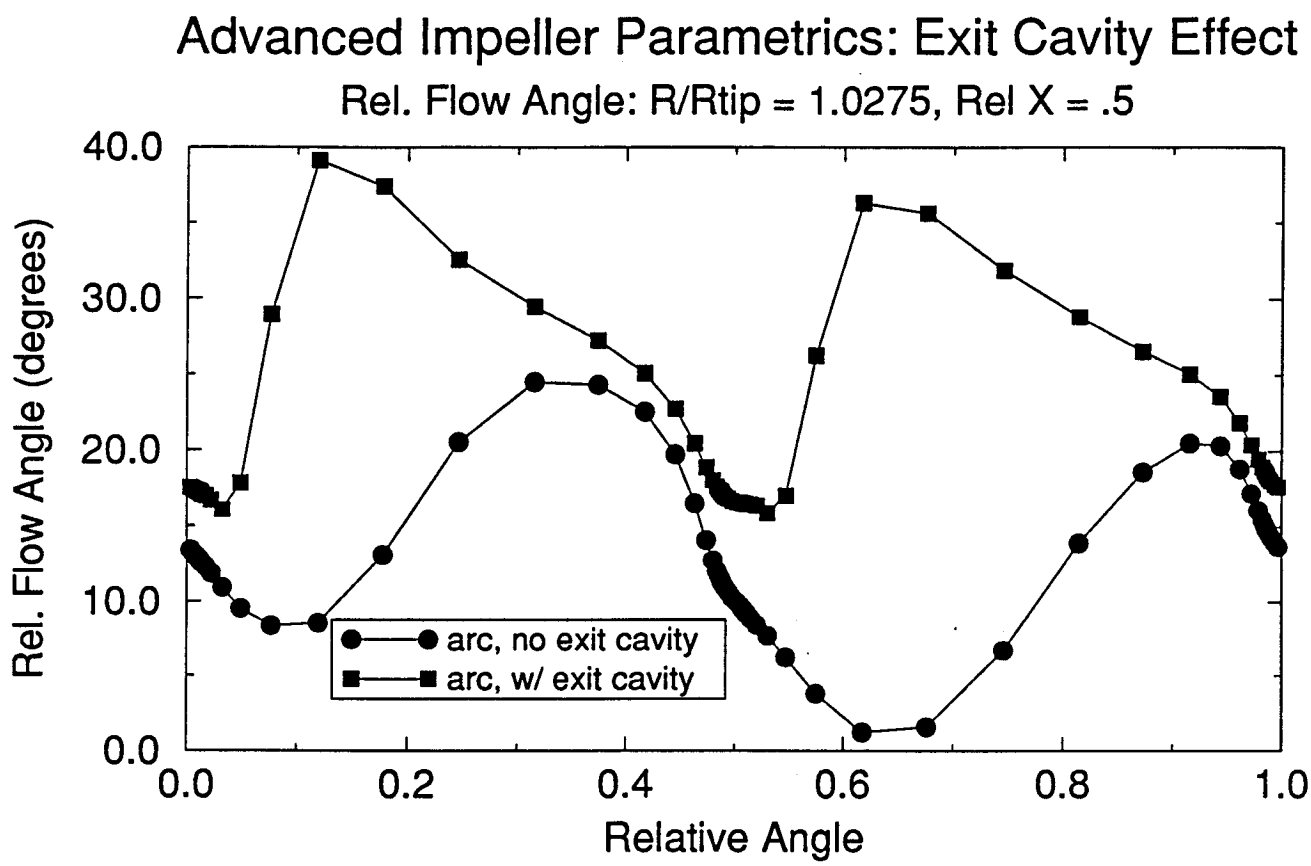

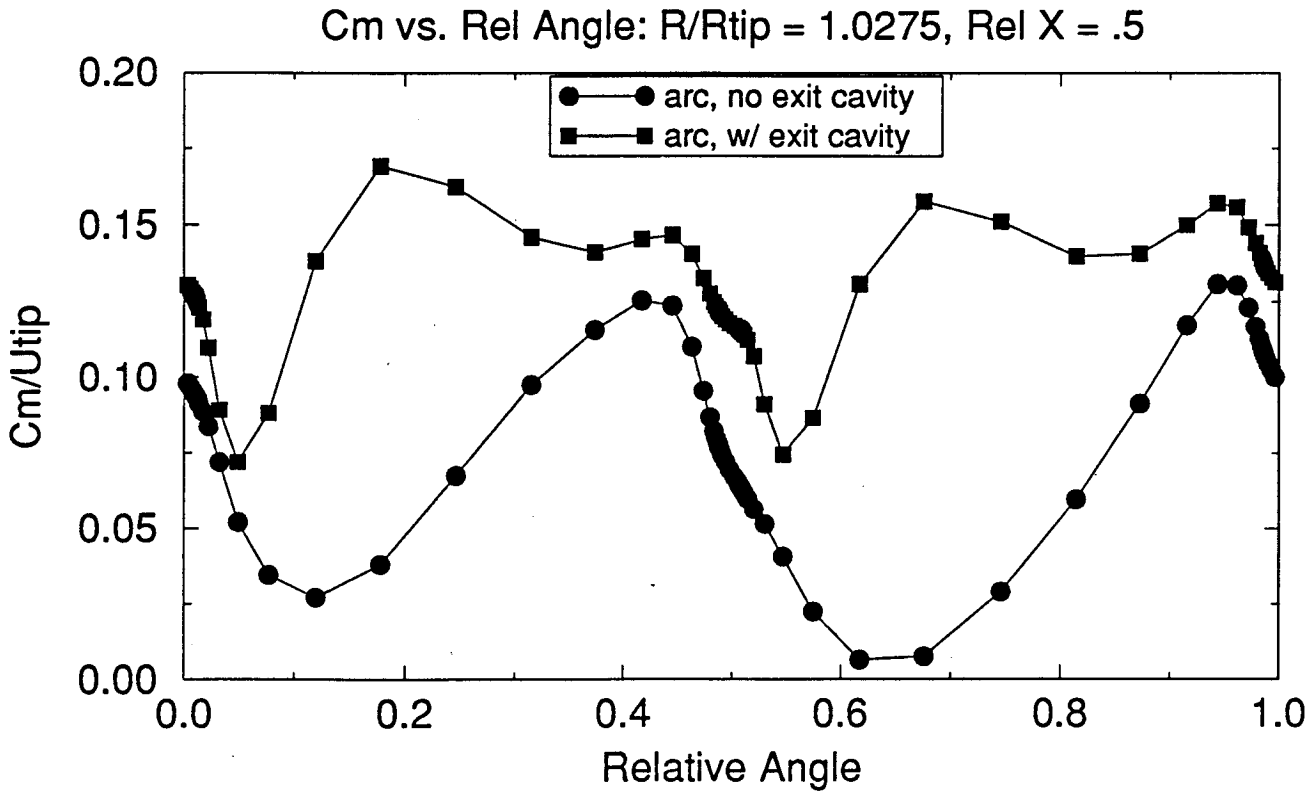

Figure 6b. Blade-to-blade impeller exit radial velocity distribution, at 50% of the blade span

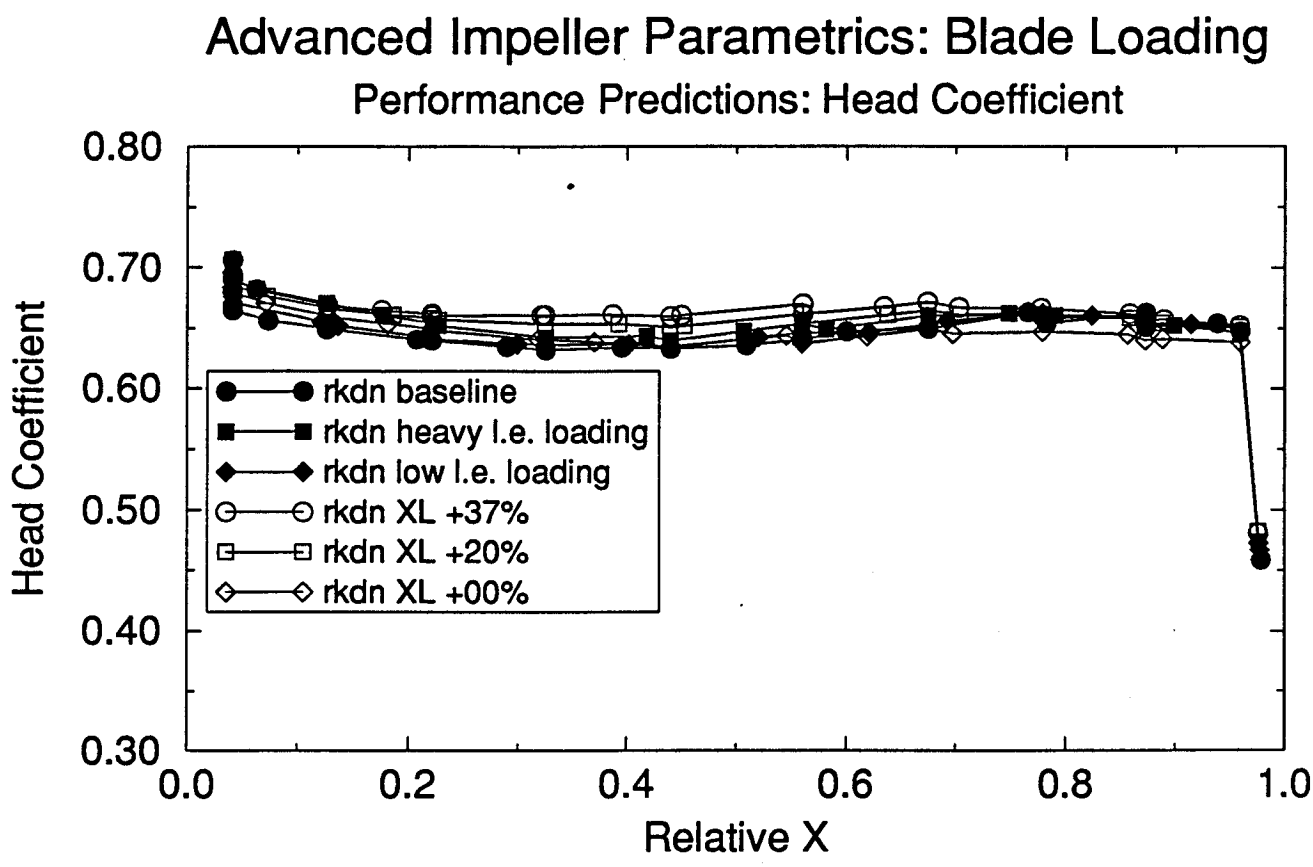

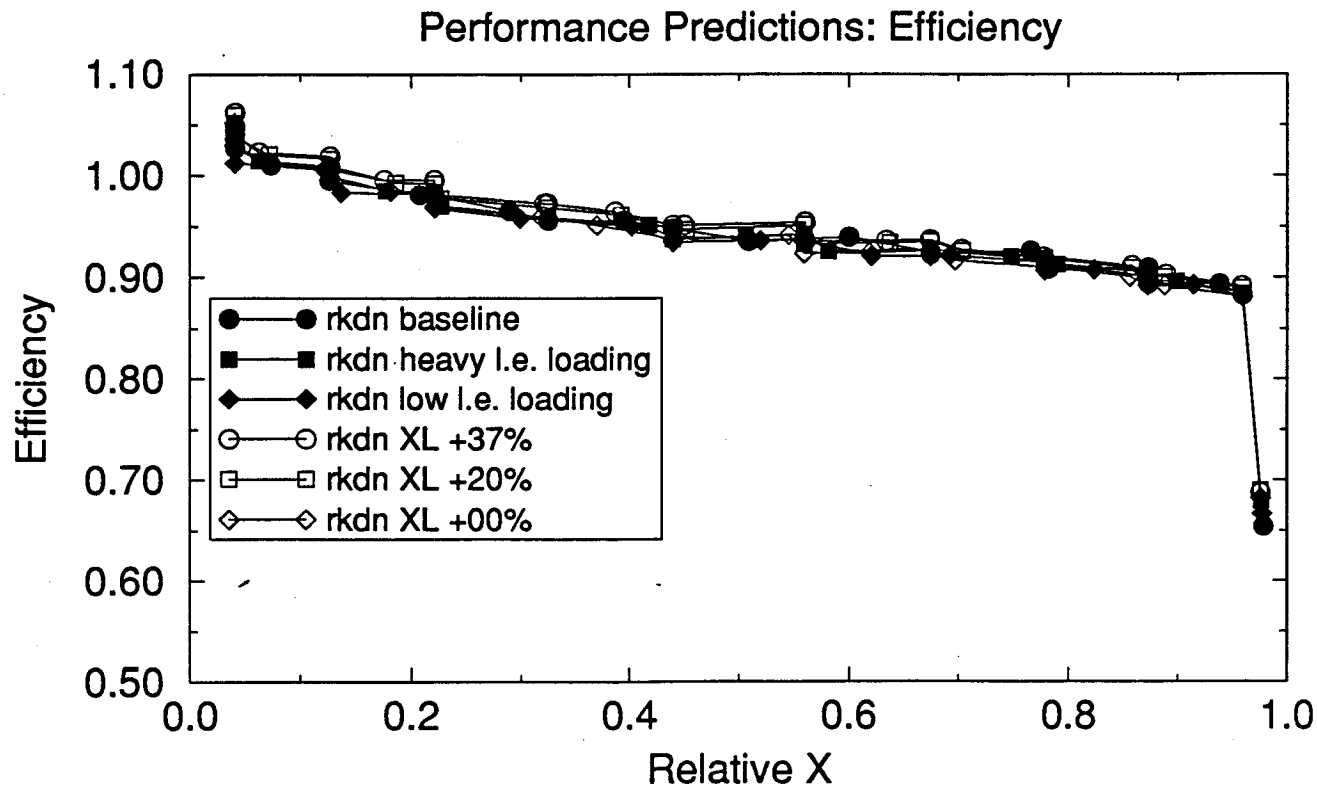

Figure 8. Performance prediction for blade loading and impeller axial length study

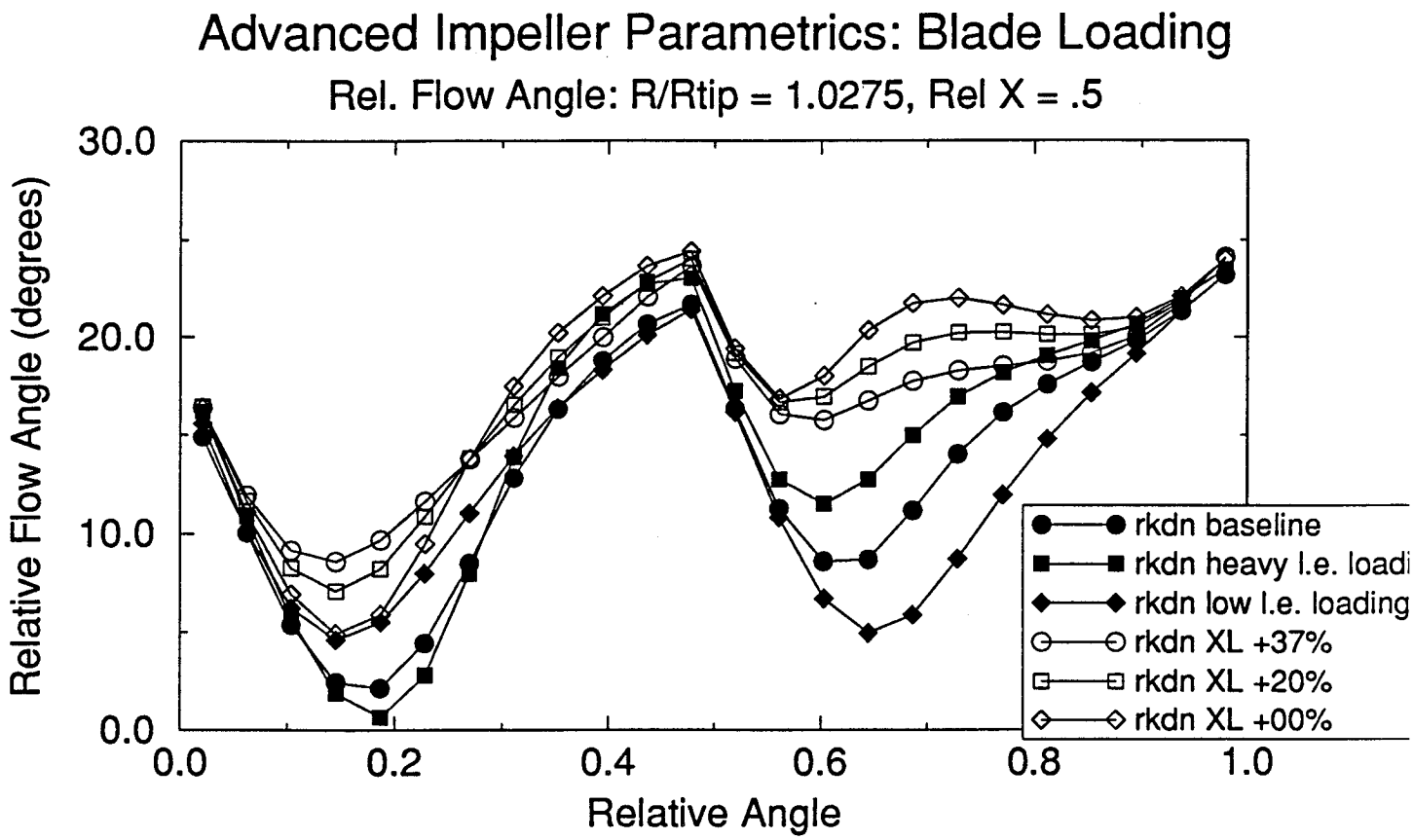

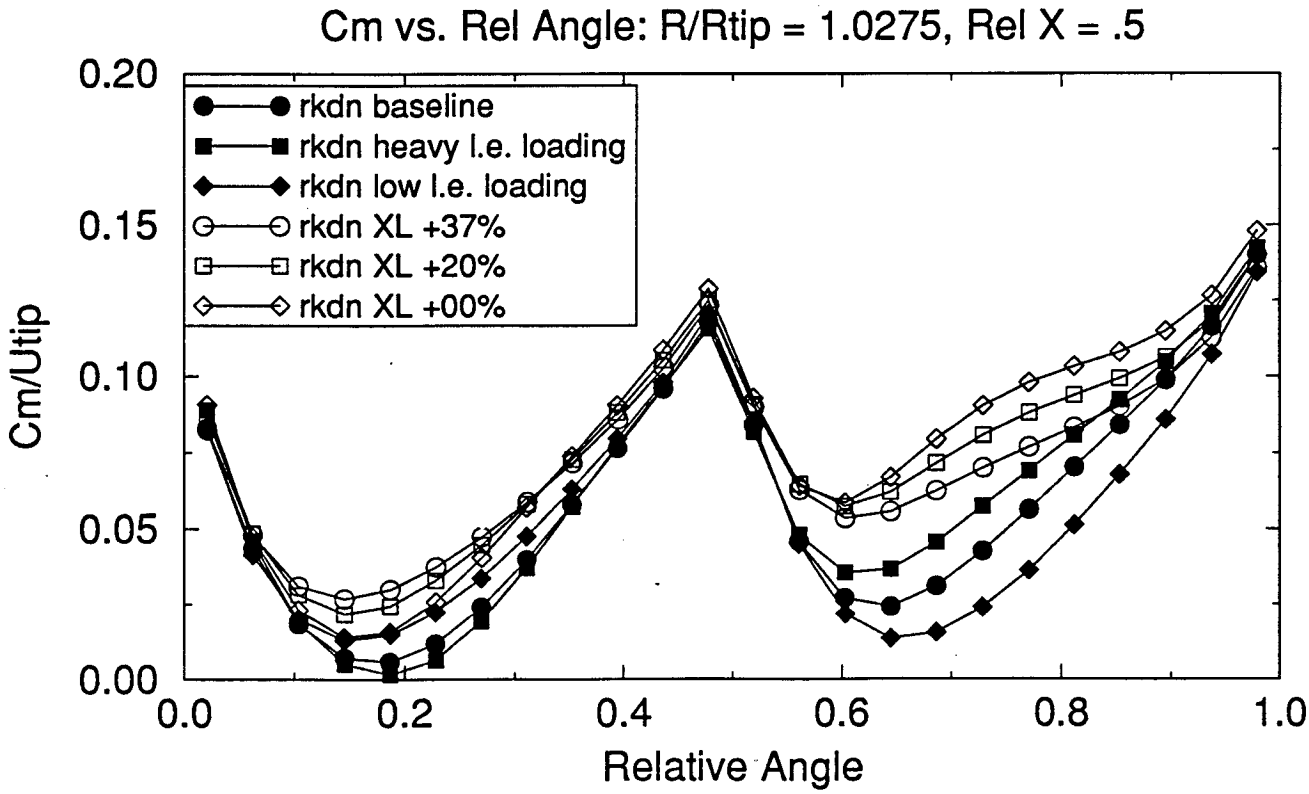

Figure 9. Blade-to-blade impeller exit radial velocity distribution at 50% of the blade span

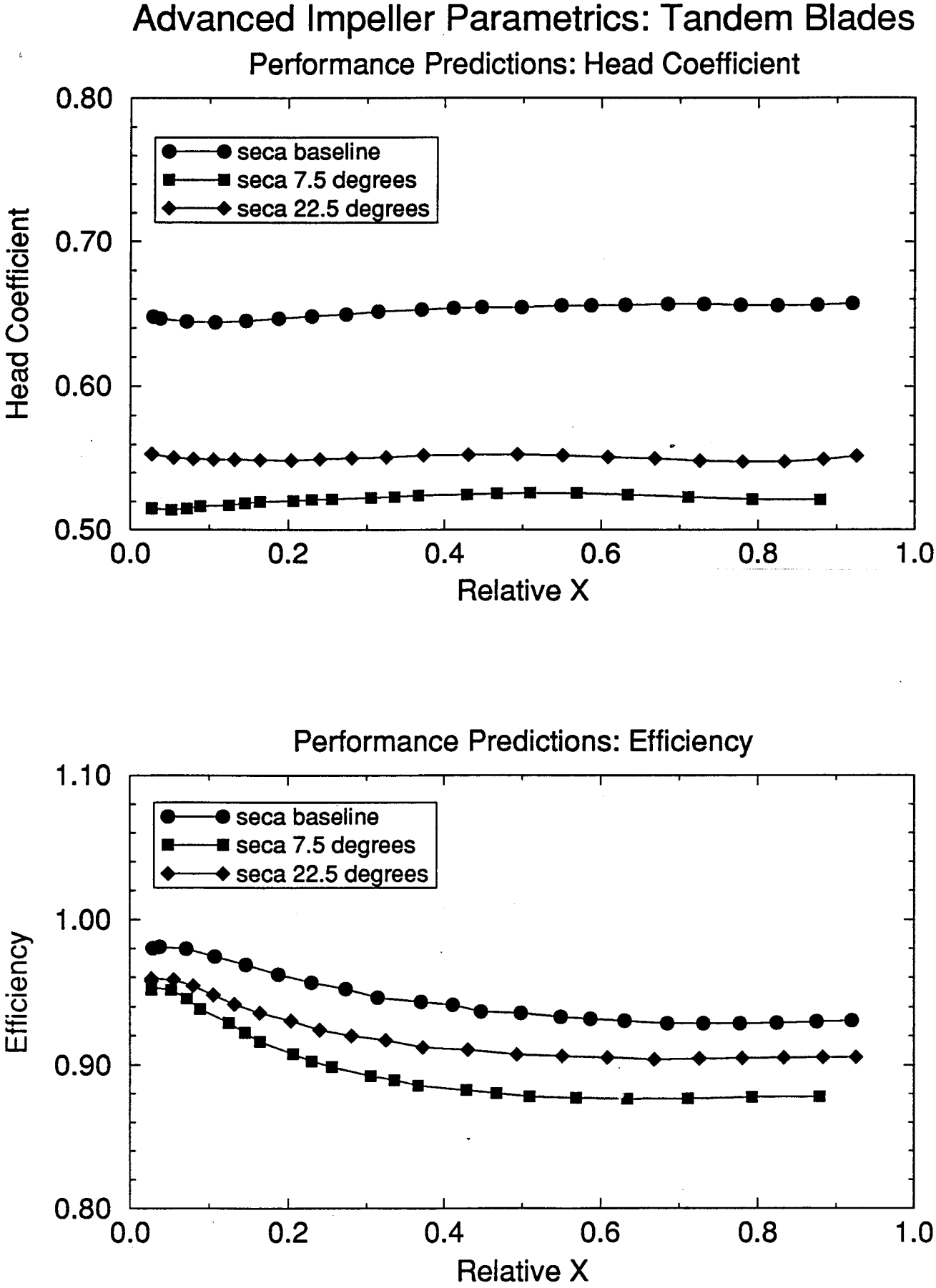

Figure 10. Performance prediction for the tandem blade study

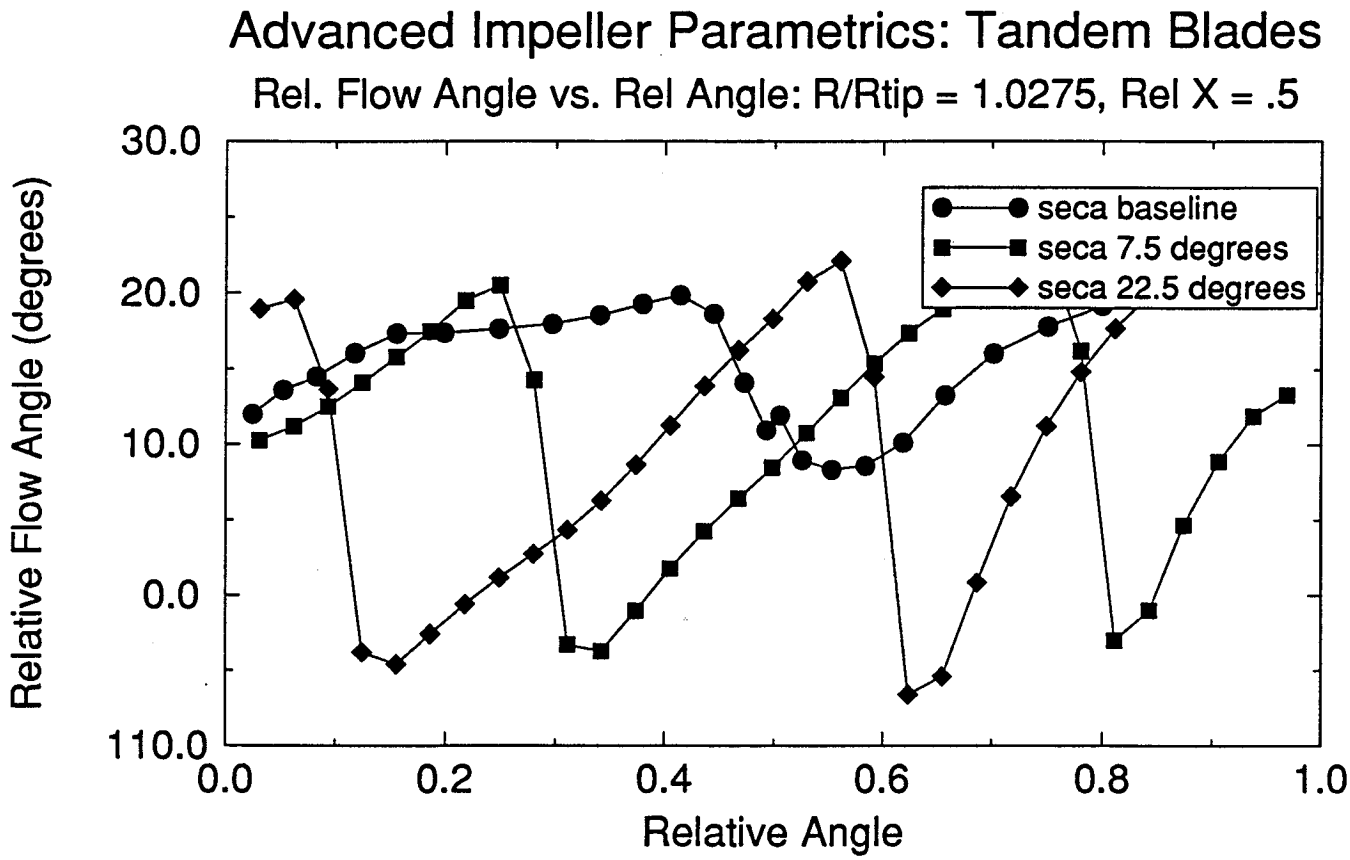

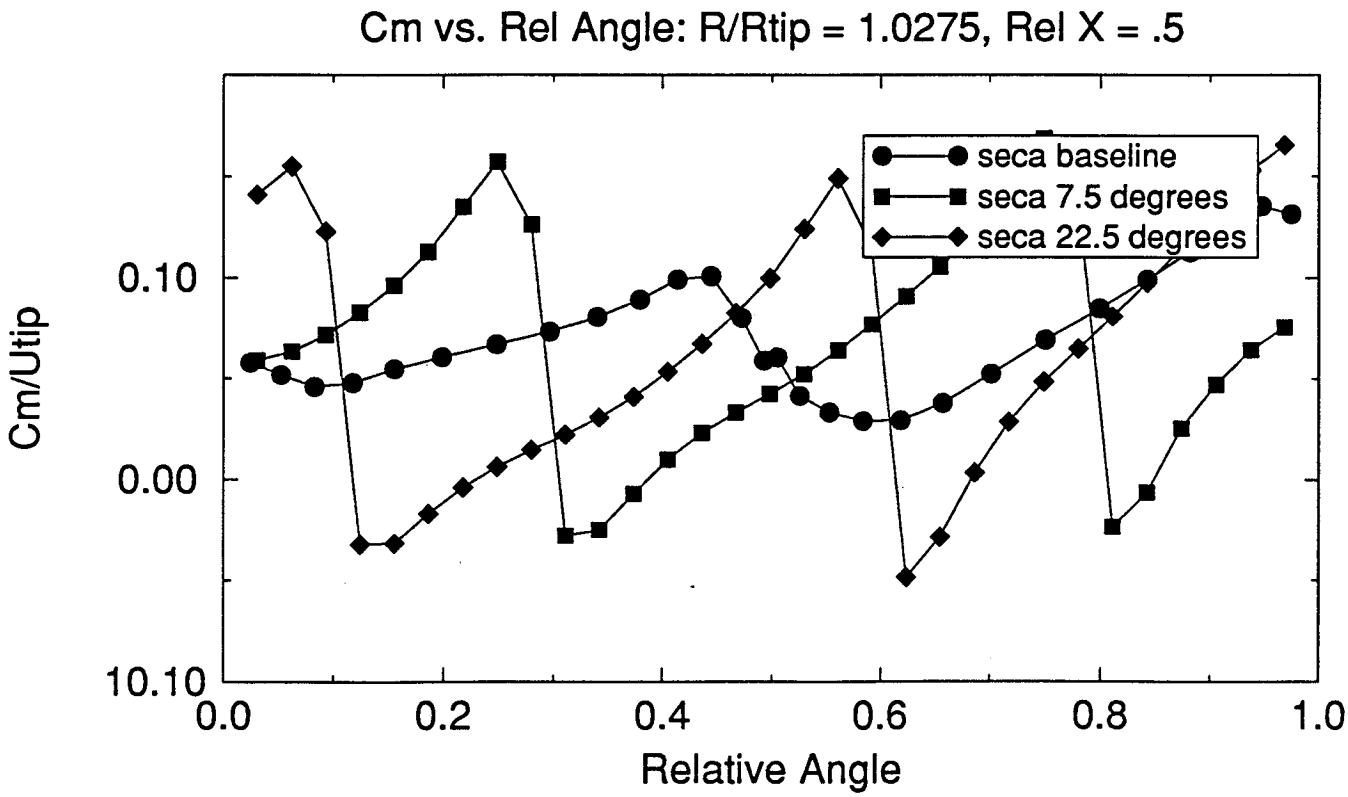

Figure 11. Blade-to-blade impeller exit radial velocity distribution at 50% of the blade span

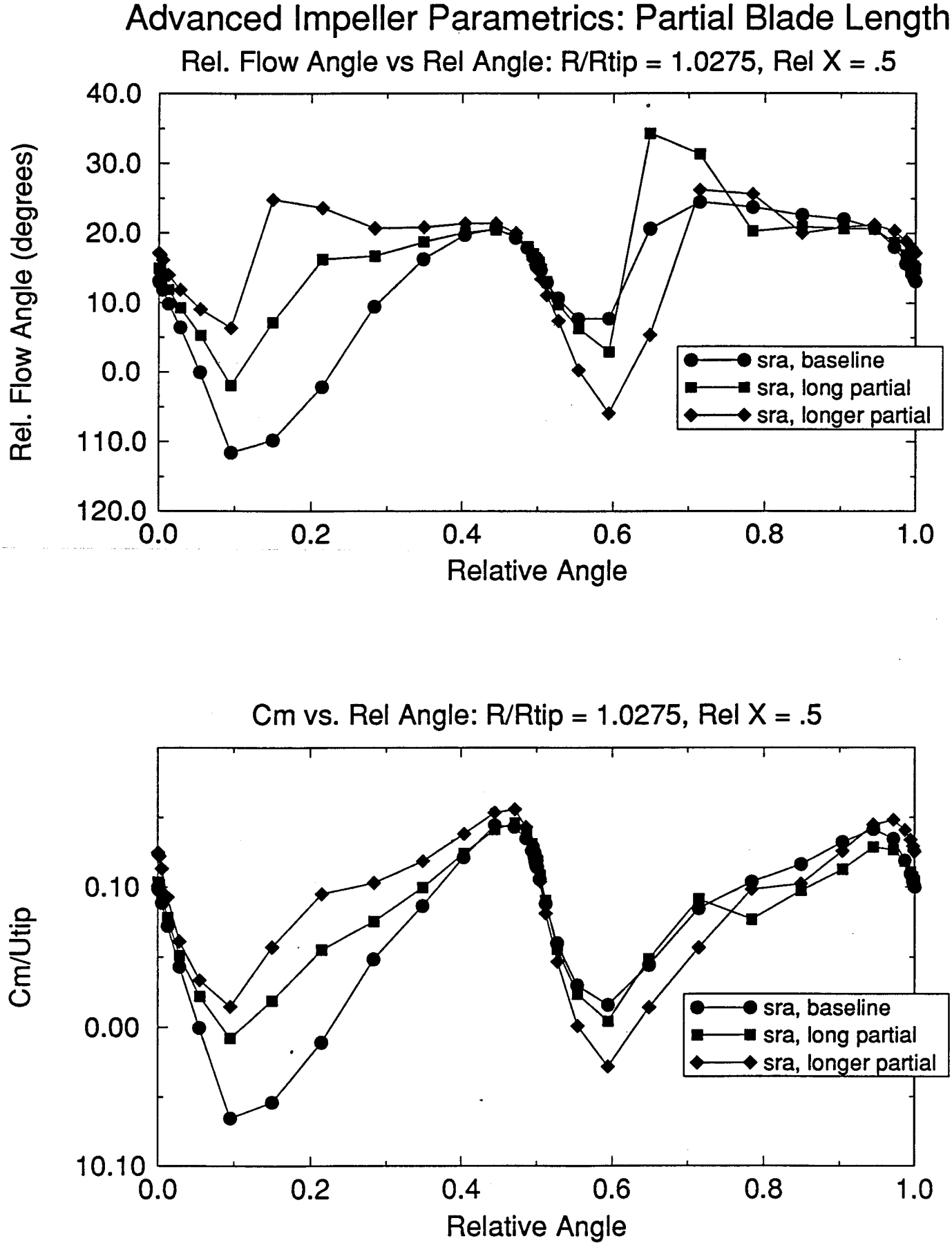

Figure 12. Blade-to-blade impeller exit radial velocity distribution at 50% of the blade span

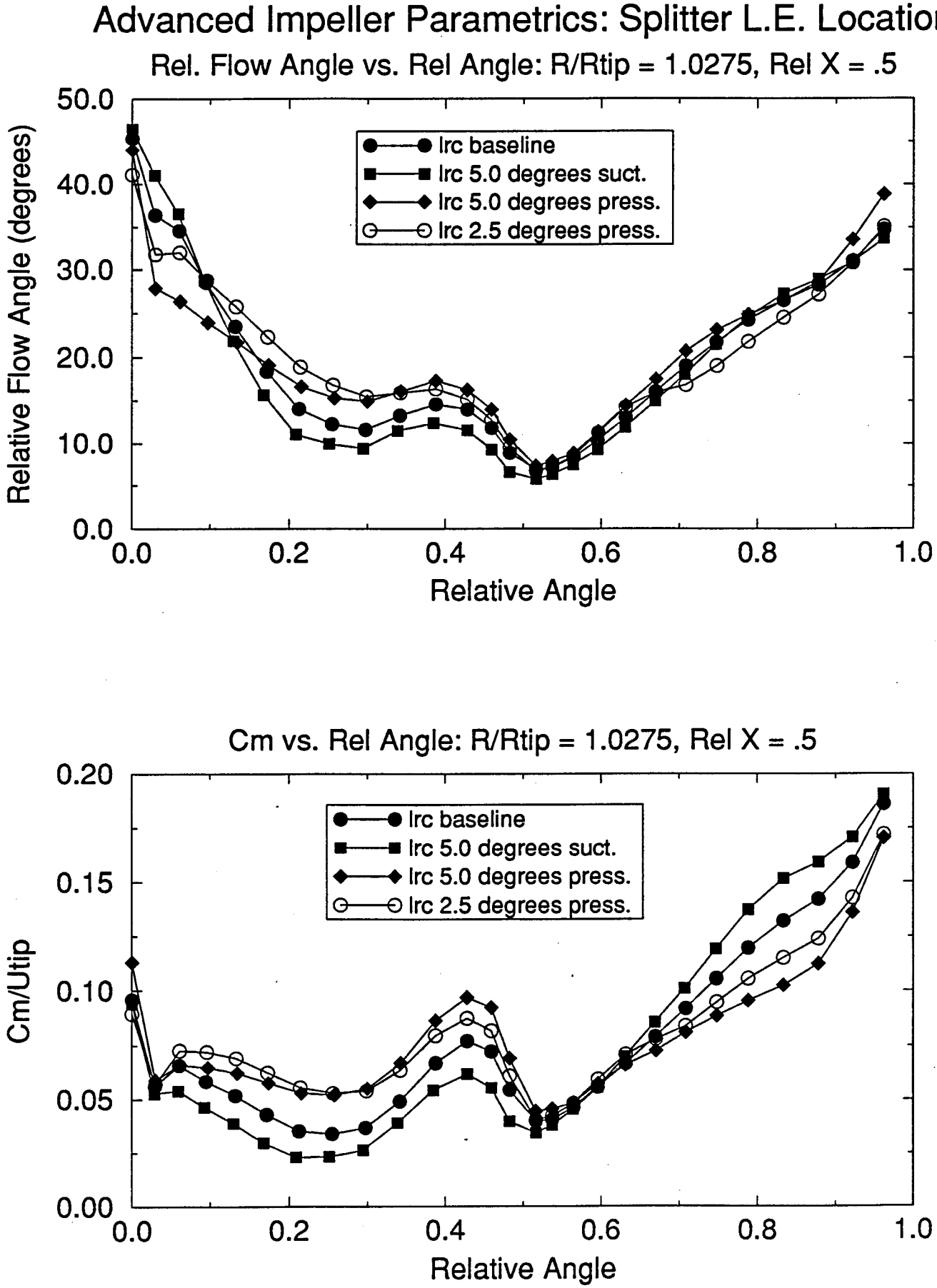

Figure 13. Blade-to-blade impeller exit radial velocity distribution at 50% of the blade span

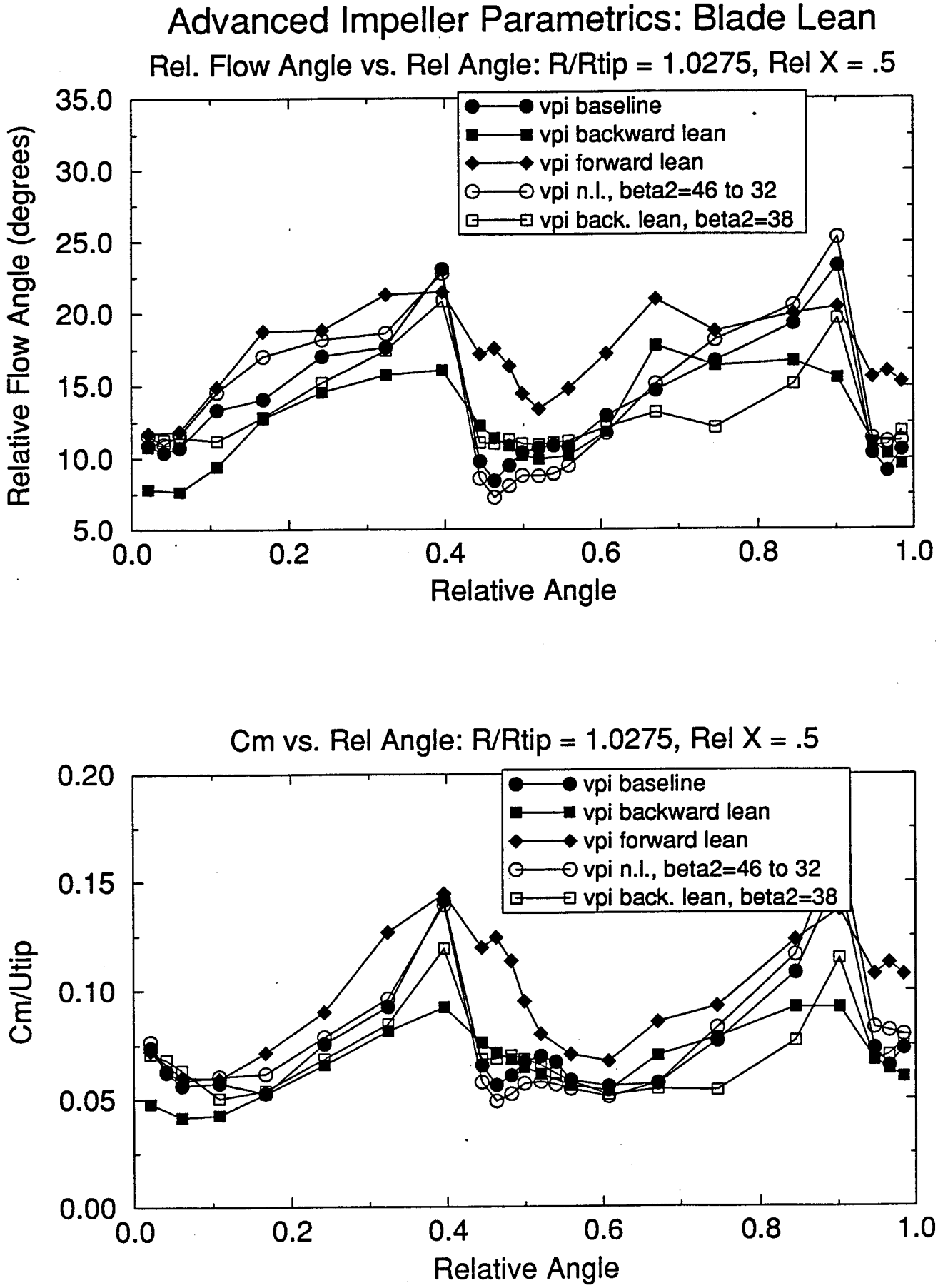

Figure 14. Blade-to-blade impeller exit radial velocity distribution at 50% of the blade span